Science Translational Medicine AAAS

Submitted Manuscript: Confidential template updated: February 28 2012

In vivo detection of cerebral tau pathology in long-term survivors of traumatic brain injury

Authors: Nikos Gorgoraptis[1]*, Lucia M. Li[1], Alex Whittington[1,2], Karl A. Zimmerman[1], Linda Mclean[3], Claire McLeod[3], Ewan Ross[1], Amanda Heselgrave[4], Henrik Zetterberg[4], Jan Passchier[2], Paul M. Matthews[1,2], Roger N. Gunn[2], Tom M. McMillan[3], David J. Sharp[1]

Affiliations:

[1]Division of Brain Sciences, Department of Medicine, Imperial College London.

[2]Invicro London.

[3]Institute of Health and Wellbeing, University of Glasgow.

[4]UK Dementia Research Institute, University College London.

*To whom correspondence should be addressed: n.gorgoraptis@imperial.ac.uk

One Sentence Summary: Flortaucipir binding in the brain is increased may years after a single traumatic brain injury, providing evidence that positron emission tomography can be used to identify tau pathology following head injury.

Abstract: Traumatic brain injury (TBI) can trigger progressive neurodegeneration, with tau pathology seen years after a single significant TBI. There are no diagnostic tests to identify this type of post-traumatic pathology *in vivo*. Here we use Flortaucipir positron emission tomography (PET) to investigate whether tau pathology is present many years after a single TBI. We relate PET results to CSF, MRI and cognitive measures of late neurodegeneration. Cerebral Flortaucipir binding was variable with many TBI patients showing increases in cortical and white matter regions. Overall, Flortaucipir binding was increased in the right occipital cortex in the TBI group when compared to healthy controls. High binding was associated with increased CSF tau and UCH-L1 levels, as well as increased MRI measures of axonal injury, a precursor of tau pathology. The results demonstrate that tau PET is a promsing approach to investigating progressive neurodegeneration associated with tauopathy following TBI.

Introduction

Traumatic brain injury (TBI) can lead to chronic neurodegeneration and dementia in later life *(1, 2)*. Deposition of hyperphosphorylated protein tau neurofibrillary tangles is a pathological hallmark of this neurodegenerative process *(3, 4)*. Since the first observations in post-mortem examinations of brain of boxers *(5)*, the pathological features and clinical correlations of tau neurofibrillary tangle deposition in chronic traumatic encephalopathy (CTE) following repetitive TBI have been increasingly well characterised *(3, 6, 7)*. However, tau deposition also occurs following a single TBI, after which abundant and widely distributed neurofibrillary tangles have been found post-mortem in approximately one-third of TBI patients *(8)*. As in Alzheimer's Disease (AD), all six isoforms of tau (including both 3- and 4-repeat isoforms) are observed in post-TBI tauopathy *(3, 4)*. However, the distribution of tau pathology after TBI follows a pattern distinct from that observed in AD, concentrating primarily in the- depths of sulci and at points of geometric inflection in the cerebral neocortex, while the medial temporal lobe is relatively spared in early disease *(8, 3)*. Although the pathogenic role of TBI as a trigger for tau aggregation is not fully understood, traumatic axonal injury appears to directly lead to tau hyperphosphorylation *(9, 10)*.

Flortaucipir ([^{18}F]AV-1451, [^{18}F]T807), a recently developed positron emission tomography (PET) radioligand for tau, enables the examination of tau pathology in vivo *(11, 12)*. Flortaucipir demonstrated potent and specific non-displaceable binding to tau neurofibrillary tangles in post-mortem human brain tissue in AD *(13–15)*. Flortaucipir is selective for tau, with no significant binding to β-amyloid, α-synuclein or TDP-43, although it also binds 'off-target' to neuromelanin- and melanin-containing cells *(13)*. *In vivo*, Flortaucipir binding is increased in AD patients with a regional pattern in keeping with the clinical phenotype *(16–18)*, cognitive profile *(16, 17)* and estimated Braak & Braak staging *(19)*. In tau mutation carriers (MAPT gene) and in AD, the distribution of in vivo Flortaucipir binding and that of post-mortem tau pathology are strongly concordant *(18, 20)*. Furthermore, in both typical AD and posterior cortical atrophy, Flortaucipir binding follows the pattern of regional atrophy as quantified by MRI *(21, 22)*.

The role of Flortaucipir in quantifying tau pathology and its distribution in long-term survivors of a single TBI has not been studied. A case report decribes a retired National Football League player exposed to repetitive TBI and manifesting progressive neuropsychiatric symptoms with increased Flortaucipir binding in bilateral cingulate, occipital, orbitofrontal and temporal

cortices *(23)*. The relationships of tau pathology to clinical outcome and biomarkers of neurodegeneration are also unclear. Of particular interest is the relationship between tau pathology and white matter microstructural changes related to traumatic axonal injury, as these will help to clarify the pathophysiological relationship between the initial injury and progressive neurodegeneration.

Here we used Flortaucipir PET to study the distribution of tau pathology in individuals at least 18 years after a single moderate-severe TBI and in healthy controls. Patients were primarily recruited from a patient cohort under follow-up at the University of Glasgow, who have previously been followed up longitudinally in terms of cognitive, wellbeing and disability outcomes *(24, 25)*. We hypothesized that: i) Flortaucipir binding would be increased in a proportion of TBI patients many years after their injury; ii) Flortaucipir binding would correlate with levels of CSF tau and other CSF and blood biomarkers of neuronal damage and neurodegeneration; iii) Flortaucipir binding would be associated with the extent and distribution of diffuse axonal injury produced by the initial injury, quantified by diffusion MRI and voxel-based morphometry (VBM); and iv) Flortaucipir binding is associated with poor long-term cognitive outcomes and disability.

Results

Participant demographic and clinical characteristics

21 patients [7 female, 14 male; median age: 49 years (range: 29 to 72)] with a history of a single moderate-severe TBI were included in the study. Participants were examined at a median time of 32 years (range: 18 to 51 years) following their injury. TBI was caused by road traffic accidents in 18 participants (86%), assault in 2 (10%) and fall from a height in 1 patient (5%). Glasgow Outcome Scale – Extended (GOS-E) median score was 6 (range: 4 to 8) at the time of assessment. In 15 patients (71%) longitudinal clinical data were also available, including GOS-E and MMSE scores obtained at a median timepoint of 16 years (range: 9 to 19 years) after the injury and 17 years (range: 15 to 19 years) before the current clinical and imaging assessment. The demographic and clinical characteristics and ApoE genotype of individual TBI patients are presented in Table 1. Nineteen patients (90%) had focal lesions with a median volume of 1634 voxels (range: 12 to 23118 voxels; Suppl. Fig. 1).

Patient	Age	Sex	TBI etiology	Time since TBI (years)	GOS-E current (change)	MMSE current (change)	ApoE
P1	56	Female	RTA	35	5 (0)	22 (-2)	ε3/ε3
P2	39	Female	RTA	28	5 (-1)	27 (-2)	ε3/ε3
P3	61	Female	RTA	35	5 (-1)	28 (-2)	ε3/ε3
P4	39	Male	RTA	32	4 (0)	28 (-1)	ε3/ε4
P5	57	Male	RTA	35	8 (0)	30 (0)	ε3/ε4
P6	54	Female	RTA	36	5 (-3)	27 (2)	ε3/ε4
P7	65	Male	Fall	31	7 (0)	30 (2)	ε3/ε4
P8	29	Female	RTA	18	7 (NA)	29 (NA)	ε3/ε3
P9	49	Male	RTA	27	5 (NA)	28 (NA)	ε2/ε3
P10	48	Male	RTA	37	6 (-2)	29 (-1)	ε3/ε3
P11	46	Female	RTA	31	8 (0)	29 (0)	ε3/ε3
P12	44	Male	RTA	29	6 (-1)	24 (-2)	ε3/ε3
P13	54	Male	RTA	32	7 (0)	29 (NA)	ε3/ε3
P14	57	Male	RTA	37	8 (0)	30 (3)	ε3/ε3
P15	54	Male	RTA	34	5 (-1)	29 (2)	ε3/ε4
P16	38	Male	RTA	19	8 (NA)	29 (NA)	ε3/ε3
P17	72	Male	Assault	51	5 (NA)	27 (NA)	ε3/ε3
P18	40	Female	RTA	31	5 (0)	23 (-6)	ε3/ε4

P19	43	Male	RTA	35	8 (0)	30 (0)	ε3/ε3
P20	55	Male	Assault	20	8 (NA)	30 (NA)	ε3/ε4
P21	43	Male	RTA	20	5 (NA)	26 (NA)	ε4/ε4

Abbreviations: ApoE: apolipoprotein E genotype; GOS-E = Glasgow Outcome Scale Extended; MMSE = Mini-Mental State Examination; NA = not available; RTA = road traffic accident; TBI = traumatic brain injury.

Table 1: Clinical characteristics of individual TBI participants.

	Outcome measure	TBI vs Healthy participants				Disabled vs Good recovery TBI subgroups			
		TBI mean (+/- SD)	Controls mean (+/- SD)	W	P	Disabled TBI subgroup mean (+/- SD)	Good recovery TBI subgroup mean (+/- SD)	W	P
Age **(years)**		49.7 (10.3)	54.2 (12.1)	80	0.16	49.9 (10)	49.3 (11,2)	35	0.29
Time since injury **(years)**		31.1 (7.6)	-	-	-	32.9 (7.4)	28.7 (7.5)	66.5	0.39
Education **(years)**		12.5 (3.6)	11.5 (2.8)	124.5	0.73	11.5 (3.2)	13.9 (3.8)	33.5	0.15
Premorbid intelligence	WTAR (scaled)	101.4 (16.4)	110.3 (10.8)	76.5	0.13	92.6 (16.1)	113.1 (6.8)	9.5	**0.002**
Cognitive impairment	MMSE (current)	26.5 (2.3)	29.5 (0.5)	4	**<0.001**	26.5 (2.3)	29.5 (0.5)	4	**<0.001**
	MMSE (change)	-0.5 (2.3)	-	-	-	-1.3 (2.4)	1 (1.4)	7	**0.041**
Logical reasoning	WASI Matrix Reasoning	22.7 (8.2)	25.2 (7)	87	0.46	18.1 (7.3)	28.9 (4.4)	8.5	**0.001**
Processing speed	Trail Making Test A (s)	39.9 (20.6)	28.9 (14.4)	153	0.079	49.7 (22.9)	27.9 (7.6)	81	**0.016**
	Trail Making Test B (s)	106.8 (69.8)	57.4 (18.3)	158	**0.049**	140.8 (75.3)	65.2 (30.6)	81	**0.016**
	Stroop Combined Baseline (s)	50.8 (10.8)	41.1 (8.5)	175	**0.017**	52.7 (12.3)	48.2 (8.6)	67	0.38
	CRT RT (ms)	579 (121)	512 (103)	160.5	0.077	645 (115)	491 (53)	94	**0.003**
Executive function	Trail Making Test B-A (s)	66.9 (56)	28.5 (8.7)	145	0.15	91.1 (63)	37.3 (26.3)	79	**0.028**
	Stroop Inhibition-Switch(s)	93 (48.7)	65.3 (20.4)	164	0.056	116.4 (52.7)	61.9 (14.2)	100	**<0.001**
	Stroop Inhibition-Switch vs Baseline (s)	71.4 (50.7)	51.8 (18.9)	145	0.25	94.6 (54.5)	40.42 (21.2)	96	**0.002**
	FrSBe-Executive; current	42.2 (8.2)	26.3 (5.7)	181.5	**<0.001**	46 (8.2)	37.1 (4.9)	89.5	**0.012**
Apathy	LARS	-21.5 (10.1)	-27.2 (6.3)	134	0.14	-17.2 (10.7)	-27.9 (4.5)	82	**0.009**
	FrSBe-Apathy; current	31.9 (9.6)	21 (5.1)	157.5	**0.005**	34.3 (10.5)	28.8 (7.8)	71	0.24
Impulsivity /	BIS	66.6 (15.8)	58.1 (6.9)	118.5	0.29	72.9 (15)	57.9 (13.2)	75	**0.039**

Disinhibition	FrSBe-Disinhibition; current	33.5 (10.3)	24.3 (5.3)	143.5	**0.028**	36.1 (11.5)	30.1 (7.7)	70.5	0.25
Verbal memory	PT Immediate Recall	18.3 (8.7)	19.8 (8.2)	102	0.61	16.4 (9.2)	20.4 (7.8)	39.5	0.32
	PT Delayed Recall	6.4 (3.8)	7.3 (3.6)	100.5	0.56	5.6 (3.9)	7.6 (3.5)	38.5	0.28
	HVLT Immediate Recall	21.2 (5.3)	25.5 (4.7)	63	**0.038**	19.4 (4.9)	23.7 (5)	25.5	**0.046**
	HVLT Delayed Recall	6.3 (3.6)	8.8 (2.5)	65.5	**0.048**	5.3 (3.9)	7.7 (2.7)	34	0.16
	HVLT RDI	9.2 (2.4)	9.9 (2)	97	0.47	8.7 (2.8)	10 (1.5)	40	0.33
Visual memory	Paired Associates Learning (z-score)	-1.47 (0.81)	-0.73 (0.92)	66	**0.043**	-1.79 (0.77)	-1.03 (0.69)	25.5	**0.036**
	BVMT Immediate Recall	16.2 (8.3)	21.7 (5.5)	63	**0.039**	10.9 (3.7)	23.3 (7.5)	7	**<0.001**
	BVMT Delayed Recall	6.8 (3.7)	9.5 (1.4)	64.5	**0.044**	4.7 (3.1)	9.6 (2.4)	12	**0.003**
	BVMT RDI	4.9 (1.3)	5.9 (0.3)	67.5	**0.026**	4.3 (1.4)	5.9 (0.3)	16	**0.004**
Visuospatial ability	Feature match test (z-score)	-1.46 (0.74)	-1.19 (0.92)	94.5	0.42	-1.88 (0.69)	-0.89 (0.31)	6	**<0.001**
Mood disturbance	HADS-Anxiety	8 (6)	3.9 (3.8)	161.5	0.069	9.9 (5.6)	5.3 (5.7)	80.5	0.063
	HADS-Depression	4.5 (4.7)	1.9 (2.5)	156	0.11	6.4 (5.1)	1.8 (2.4)	86.5	**0.022**

Abbreviations: BIS = Barratt Impulsivity Scale; BVMT = Brief Visuospatial Memory Test; CRT = Choice reaction time; PT = People's Test; FrSBe = Frontal Systems Behavior Scale; HADS = Hospital Anxiety and Depression Score; HVLT = Hopkins Verbal Learning Test; LARS = Lille Apathy Rating Scale; MMSE = Mini-mental State Examination; ms = milliseconds; RDI = Recognition Discrimination Index; RT = Reaction time; s = seconds; SD = Standard deviation; WASI = Wechsler Abbreviated Scale for Intelligence; WTAR = Wechsler Test of Adult Reading.

Table 2: Demographic and neuropsychological comparisons between TBI patient and healthy control groups, as well as between disabled TBI and good recovery TBI subgroups. Independent sample Mann-Whitney-Wilcoxon test W and P-values (P<0.05 in bold) are provided for comparisons between groups and subgroups.

11 healthy controls [5 female, 6 male; median age: 57 years (range: 29 to 72)] of similar educational background and estimated premorbid intelligence to the TBI participants were also examined. The demographic characteristics of the TBI and control groups are presented in Table 2.

We divided TBI participants into a good recovery and a disabled subgroup based on their Glasgow Outcome Scale – Extended scores (disabled subgroup: GOS-E≤6; good recovery subgroup: GOSE>6). Twelve participants [5 female, 7 male; median age: 48.5 years (range: 39 to 72)] with a median GOS-E of 5 (range: 4 to 6) were included in the disabled subgroup and 9 TBI participants [2 female, 7 male; median age: 54 years (range: 29 to 65)] with a median GOS-E of 8 (range: 7 to 8) were included in the good recovery subgroup. Longitudinal clinical data were available for 9 patients (75%) in the disabled and 6 patients (67%) in the good recovery group. The demographic characteristics of these subgroups are presented in Table 2.

Neuropsychological performance

When compared to healthy controls, TBI participants manifested impairments on multiple cognitive domains including processing speed, executive function, motivation, inhibition, verbal and visual memory (Table 2), in a neuropsychological profile typical of TBI. The good recovery TBI subgroup performed better than the disabled subgroup on several cognitive domains including logical reasoning, processing speed, executive function, motivation, inhibition, verbal memory, visual memory and mood assessment (Table 2). As shown in Table 2, there was evidence of cognitive decline on longitudinal assessment (average -1.3 point on MMSE) in the disabled TBI subgroup while the good outcome TBI subgroup showed improvement of cognitive performance over time (average 1 point on MMSE), with longitudinal change being significantly different between the TBI subgroups.

Flortaucipir binding in individual TBI patients

To obtain a quantitative assesment of Flortaucipir binding and its distribution in the brain in individual TBI patients, voxelwise z-scores of MNI registered Flortaucipir binding potential (BP_{ND}) images were derived for each patient versus the healthy control group. This approach allows areas of increased binding to be identified in the individual, relative to variations in binding seen in healthy subjects. As illustrated in Fig. 1, several TBI participants had increased Flortaucipir binding in a patchy cortical and subcortical distribution (Fig. 1: P1 to P8 and P10). In contrast, other TBI participants had similar Flortaucipir BP_{ND} to that of healthy controls (Fig. 1: P17 to P22).

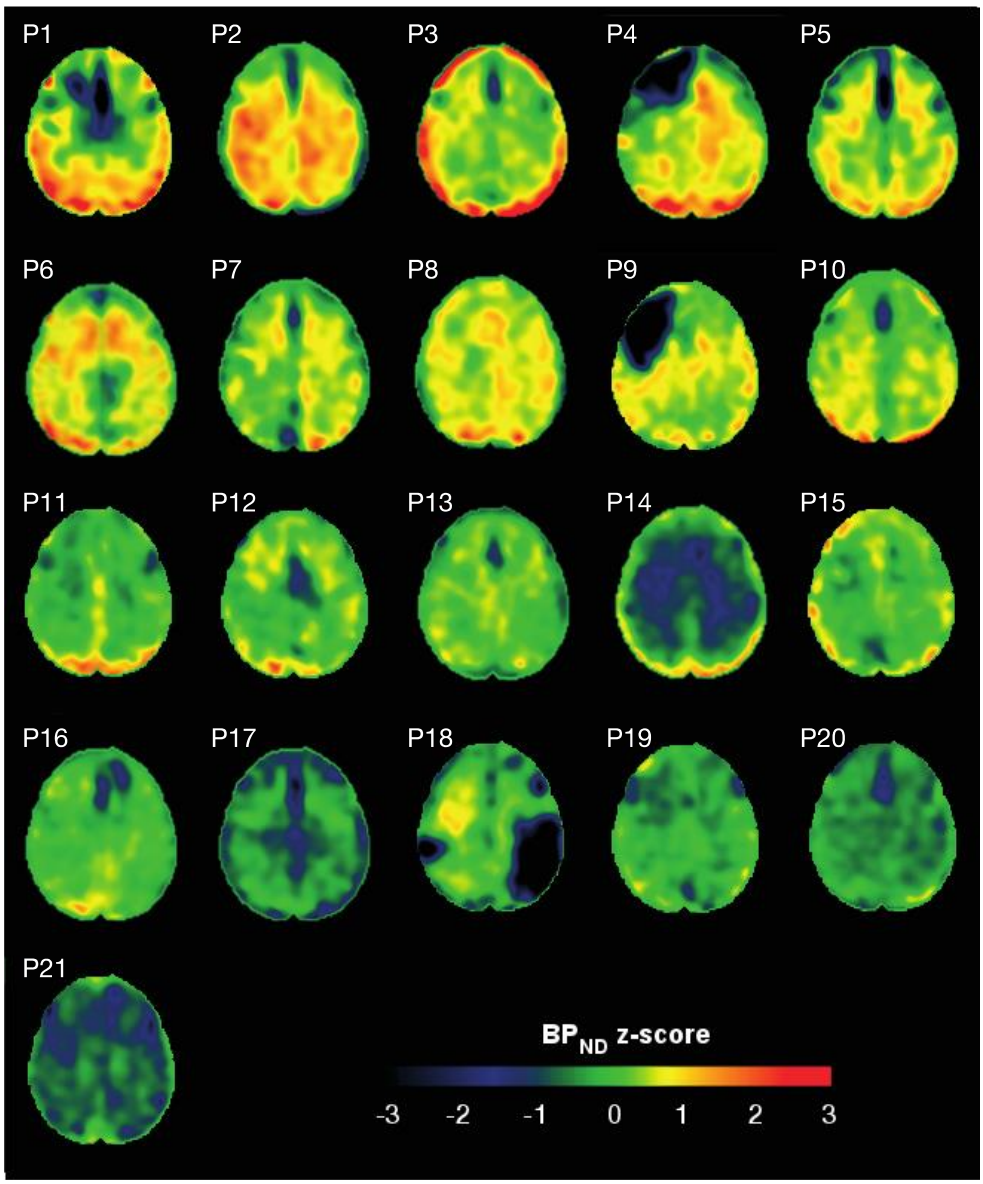

Fig. 1: Flortaucipir BP_{ND} z-score maps for each TBI individual compared voxelwise to healthy controls. TBI participants are presented in descending order of number of voxels with Flortaucipir BP_{ND} z>1.645 (see Figure 2). Axial images are displayed in radiological convention at MNI coordinate 55. Patchy cortical and subcortical increase in tracer uptake is observed in some patients, most consistently in the lateral occipital cortex (P1 to P8 and P10), while other patients show similar BP_{ND} values as controls (P17 to P21). The corresponding clinical characteristics are presented in Table 1.

The number of voxels with high BP_{ND} (z>1.645; corresponding to one-tailed P<0.05) was used to measure the spatial extent of increased Flortaucipir signal in individual patients (Fig. 2). TBI participants had a median 841 voxels above threshold (range: 0 to 15809). For comparison, voxelwise z-scores were also derived for each healthy control versus the rest of the control group. In controls, the median number of voxels above threshold was 4 (range: 0 to 253; Fig. 2).

Eight TBI participants (38%) had >2000 voxels (equivalent to 16 cm^3 of brain volume) above threshold indicating spatially extensive Flortaucipir signal increase, while a further 7 (33%) showed increased signal of more spatially limited extent (254-1999 voxels, Fig. 2). The remaining 6 TBI patients (29%) had less than 253 voxels above threshold, falling within the range of the healthy control group. There was no difference in the spatial extent of high Flortaucipir signal when comparing between disabled and good functional outcome subgroups (Mann-Whitney-Wilcoxon W=68.5, P=0.32).

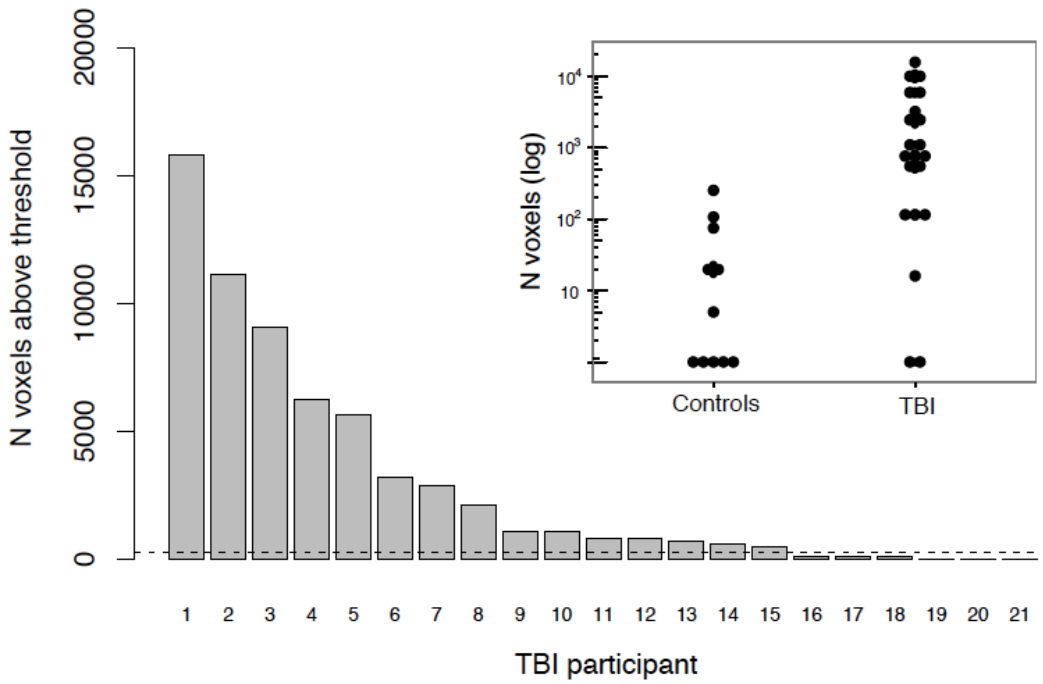

Fig. 2: Spatial extent of increased Flortaucipir signal in TBI. Spatial extent of Flortaucipir binding is expressed as the number of voxels with Flortaucipir BP_{ND} z>1.645 for each TBI patient compared to the healthy control group. The dotted line represents the number of voxels above threshold in the healthy control subject with the maximum number of voxels above that threshold (compared to the rest of the controls). The inset figure shows the number of voxels above threshold (in logarithmic scale) in TBI and healthy controls.

Reduced Flortaucipir binding within focal lesions in TBI

Flortaucipir binding within focal lesions was significantly reduced when compared to non-lesioned cerebral areas (Wilcoxon signed-rank V=22, P=0.002). Areas of markedly reduced Flortaucipir uptake (in black) in Fig. 2 correspond to focal lesions in individual patients (cf Suppl. Fig. 1).

Increased Flortaucipir binding in the TBI patient group vs. healthy controls

Flortaucipir BP_{ND} was next compared between TBI and healthy control groups, excluding lesioned areas and also the striatum where off-target binding is observed with this tracer (Suppl. Fig. 1). Flortaucipir binding was significantly higher in TBI participants than in healthy controls in the right lateral occipital cortex (Fig. 3 inset; P<0.05, adjusted for multiple comparisons). There was no significant difference in Flortaucipir binding when comparing between the disabled (GOS-E≤6) and good

outcome (GOS-E>6) TBI subgroups. When each of the TBI subgroups was independently compared to healthy controls, significantly increased Flortaucipir binding was found in both TBI subgroups, in the same right lateral occipital area (Fig. 3). There were no areas of significantly decreased binding in the TBI group or subgroups compared to healthy controls.

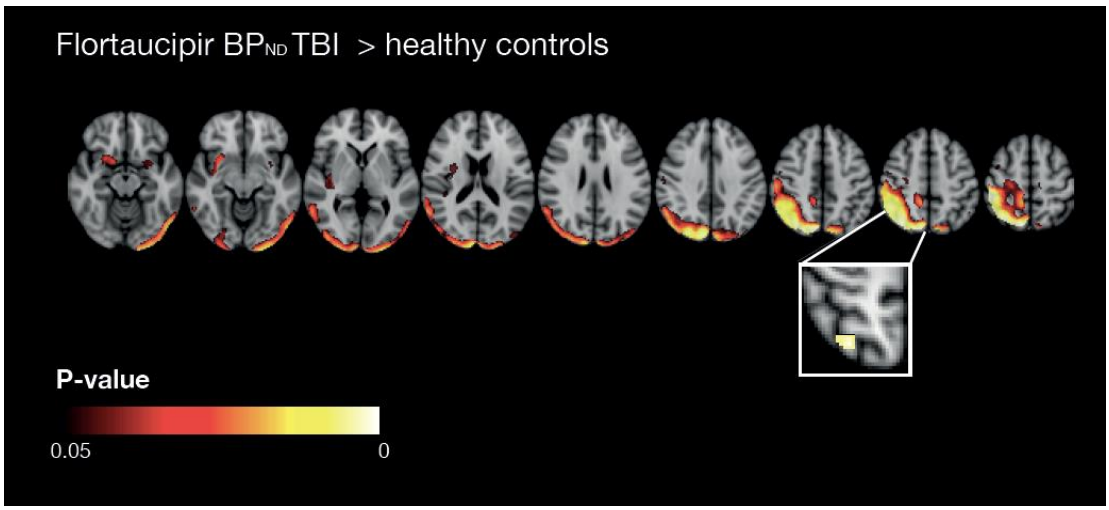

Fig. 3: Increased Flortaucipir BP_{ND} in TBI compared to healthy controls. Voxels with increased Flortaucipir uptake in TBI at P<0.05, not adjusted for multiple comparisons, are shown on axial slices for illustration. Flortaucipir binding was increased in TBI in a small cluster of voxels in the right parietal cortex (inset, P<0.05, corrected for multiple comparisons).

Cortical Flortaucipir correlates with CSF tau and UCH-L1 in TBI

Next, CSF and serum biomarkers of neurodegeneration and neuronal damage, including total tau, UCH-L1, NFL, GFAP and S100 were assessed in TBI and healthy controls and their relationship with Flortaucipir uptake was examined. CSF data was available from 19 TBI participants and 10 healthy controls. In TBI, increased CSF tau was significantly correlated with increased Flortaucipir BP_{ND} in the cerebral cortical grey matter (Spearman ρ=0.53, P=0.023; Fig. 4A). CSF tau did not correlate with Flortaucipir uptake in healthy controls. Plasma tau levels did not show significant correlations with Flortaucipir uptake in either TBI or healthy controls. Tau levels in CSF and plasma were not different between TBI and healthy control groups.

UCH-L1 in the CSF in TBI participants also positively correlated with Flortaucipir BP_{ND} in the grey matter (Spearman ρ=0.52, P=0.023; Fig. 4B), but not in

the white matter. There was no significant association between plasma UCH-L1 and Flortaucipir uptake in TBI. In healthy controls, there were no significant associations between Flortaucipir uptake and UCH-L1 in the CSF or plasma. There was no statistically significant difference between TBI and control groups in UCH-L1 levels. There were also no statistically significant associations between Flortaucipir BP_{ND} and NFL, GFAP or S100 in TBI or healthy controls and no significant dfference between TBI and control groups in the CSF or plasma.

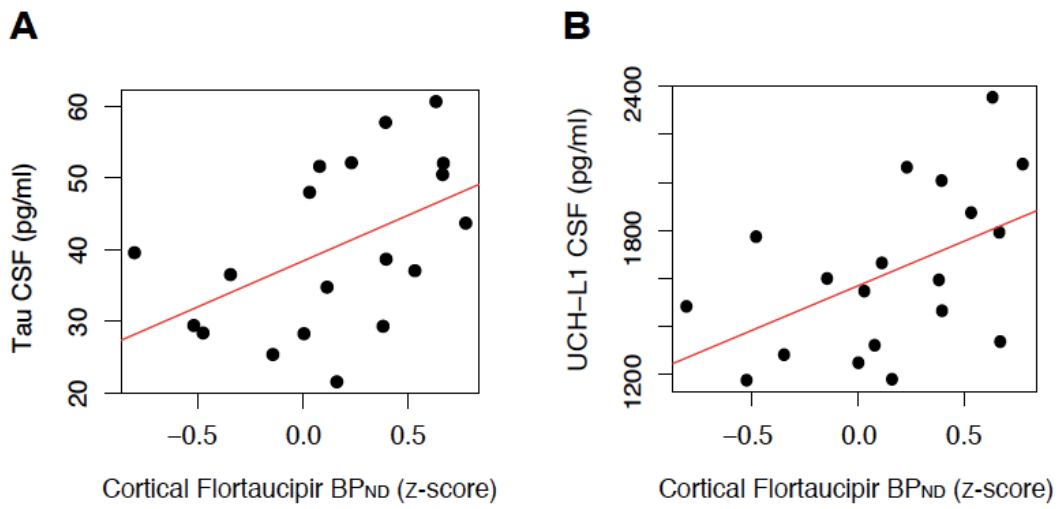

Fig. 4: Flortaucipir and CSF biomarkers in TBI. Flortaucipir BP_{ND} in the cerebral grey matter is positively correlated with tau and UCH-L1 CSF levels in TBI participants.

Flortaucipir spatial extent correlates with white matter damage in TBI

Next, we investigated the relationship between Flortaucipir binding and structural brain injury produced by TBI *(26).* White matter integrity measured by fractional anisotropy (FA) was significantly reduced in TBI when compared to healthy controls (Mann-Whitney-Wilcoxon W=44, P=0.004), in keeping with the presence of traumatic axonal injury (TAI) in TBI. Tissue density measured by voxel based morphometry (VBM) was also significantly reduced in the non-lesioned white matter in TBI (Mann-Whitney-Wilcoxon W=61, P=0.031). Tissue density in the non-lesioned grey matter was not significantly different between TBI and healthy control groups (W=113, P=0.94).

The spatial extent of Flortaucipir binding (number of voxels with BP_{ND} z>1.645) correlated with the degree of white matter damage see in TBI patients. The number of voxels showing increased Flortaucipir binding was negatively correlated with both average FA (Spearman ρ=-0.48, P=0.027) and average white matter density (Spearman ρ=-0.46, P=0.037), in keeping with a relationship between more tau pathology in the cortex with microstructural white matter disruption. There was no relationship between Flortaucipir binding and gray matter tissue density.

White matter damage seen in areas of increased Flortaucipir binding

We next examined whether greater white matter pathology was seen in areas of increased Flortaucipir binding. As the location of post-traumatic damage varies from patient to patient, we defined areas of high and low Flortaucipir signal (BP_{ND} z > or < 1.645) in each patient. Within the white matter, eight patients showed low Flortaucipir signal within the white matter they were excluded from these analyses. Significantly lower FA (Figure 5A-B; Wilcoxon signed-rank V=19, P=0.018) and white matter density (Figure 5C-D; Wilcoxon signed-rank V=17, P=0.025) was seen in areas of high Flortaucipir binding compared to areas where binding was not increased, demonstrating realtively high Flortaucipir binding in areas of post-traumatic white matter damage. The corresponding VBM analysis for grey matter density did not reveal significant differences in gray matter density in areas of high or normal Flortaucipir binding.

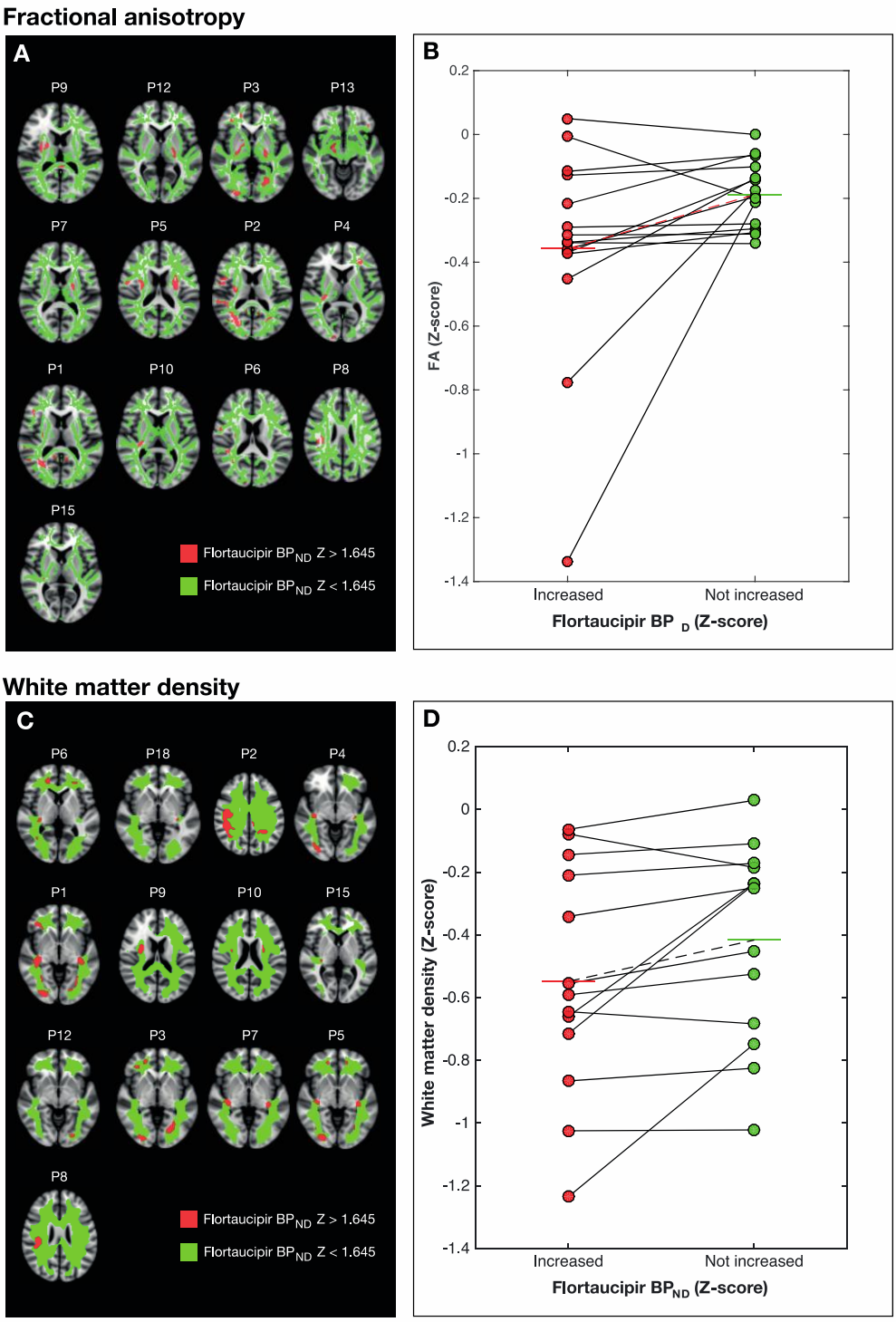

Fig. 5: Co-localisation of increased white matter Flortaucipir BP_{ND} with white matter microstructural changes in TBI. Skeletonized FA **(A)** and white matter density **(B)**, standardized against controls, were compared within subject between areas of increased Flortaucipir binding (in red) and areas where binding was not increased (in green). A representative axial slice for each patient shows the spatial distribution of the white matter areas compared and images are presented in order of greatest to smallest effect size (greatest decrease in FA or white matter density z-score in high Flortaucipir areas shown top left). Both FA z-scores **(B)** and white matter density z-scores **(D)** are lower within areas of increased Flortaucipir binding, defined as BP_{ND} Z > 1.645**.**

Cortical Flortaucipir binding and white matter microstructural damage

Next, we examined whether Flortaucipir BP_{ND} within the right lateral occipital cortical area where Flortaucipir signal was significantly increased in TBI vs controls (Fig. 3) was associated with white matter tract FA. Increased right lateral occipital Flortaucipir binding was associated with reduced FA in remote white matter regions, including association, comissural and projection tracts in the ipsilateral and contralateral hemisphere (Fig. 6A&B and Supplementary Table S1). Correlations were observed in the genu and body of the corpus callosum, as well as in several association tracts within the ipsilateral (right) hemisphere, including the cingulum bundle, inferior longitudinal fasciculus, uncinate fasciculus and anterior thalamic radiation, but not in the contralateral hemisphere. Higher cortical Flortaucipir BP_{ND} was associated with significantly reduced tissue density in remote white matter regions including the corpus callosum and right prefrontal white matter (Fig. 6C). A similar analysis for grey matter density did not show any significant association between Flortaucipir BP_{ND} within the lateral occipital cluster and cerebral cortical grey matter density.

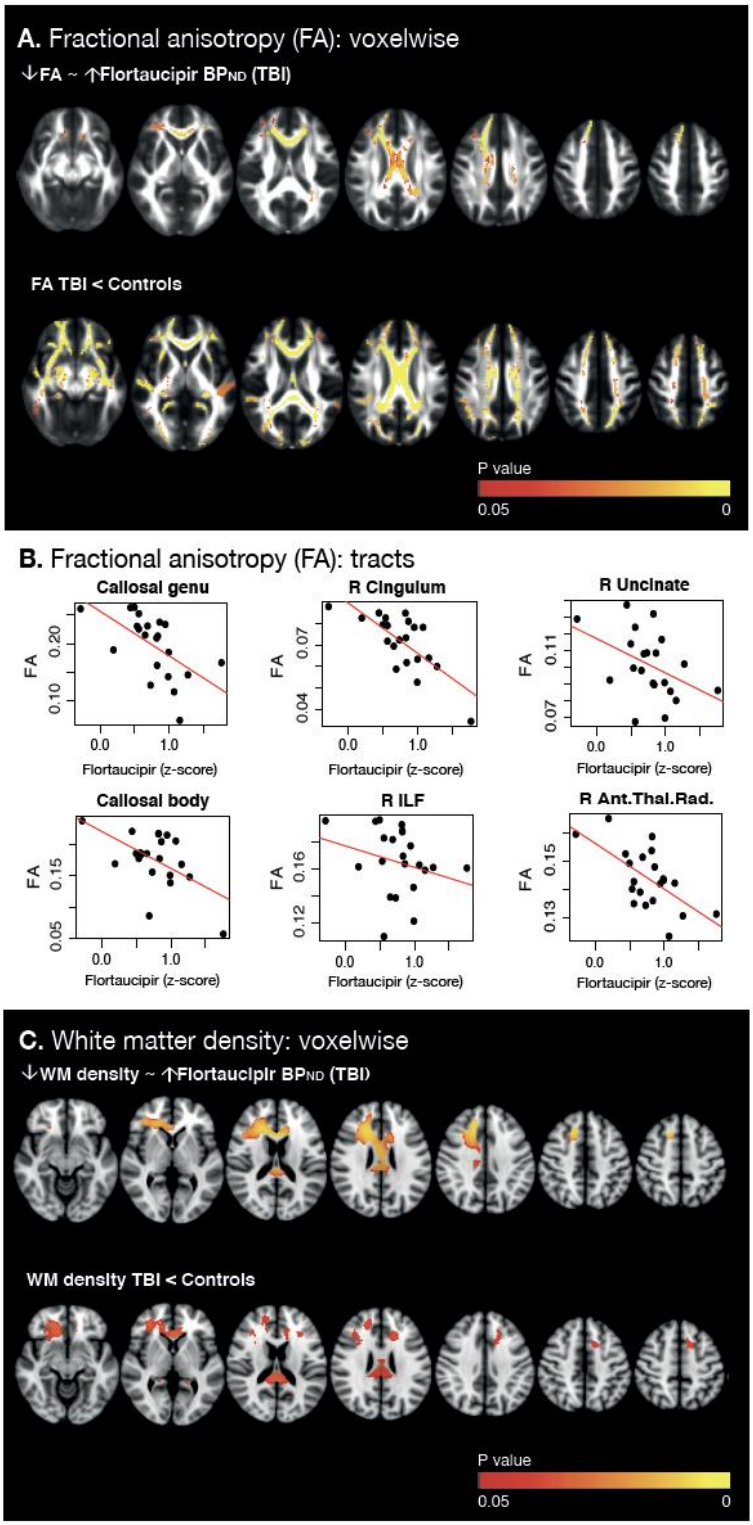

Fig. 6: Increased cortical Flortaucipir binding in the right lateral occipital area is associated with microstructural white matter damage in TBI. A) Increased Flortaucipir BP_{ND} in the right lateral occipital cortex in TBI patients was associated with reduced diffusion MRI-derived fractional anisotropy (FA) in remote white matter tracts (upper panel), partly overlapping with white matter tracts of reduced FA in TBI when compared to controls (lower panel). **B)** Flortaucipir BP_{ND} in the right lateral occipital cortex in TBI patients correlated negatively with average skeletonized FA within the genu and body of the corpus callosum as well as within the cingulum bundle, inferior longitudinal fasciculus, anterior

thalamic radiation and uncinate fasciculus in the right hemisphere. Correlation coefficients and P-values presented in Table 3. **C)** Increased Flortaucipir BP_{ND} in the right lateral occipital cortex in TBI patients is associated with reduced voxel-based morphometry-derived white matter density in the corpus callosum and right prefrontal area (upper panel). This distribution partly overlaps with areas of white matter atrophy in TBI when compared to controls (lower panel). Results presented in radiological convention, color maps represent P values <0.05 adjusted for multiple comparisons.

Flortaucipir PET and neuropsychological measures in TBI

There were no significant correlations between average Flortaucipir BP_{ND} in the cerebral grey or white matter and any clinical or neuropsychological measures in the TBI participants (all P>0.05, false discovery rate-adjusted, Supplementary Table S2). Furthermore, there was no statistically significant correlation between the spatial extent of high Flortaucipir signal in TBI patients (number of voxels above BP_{ND} z>1.645) and any clinical or neuropsychological measures in TBI (Table S1; all P>0.05, false discovery rate-adjusted).

Interaction between ApoE genotype and age on Flortaucipir cortical uptake

There were no differences between TBI participants with at least one ApoE ε4 allele and those without an ApoE ε4 allele in Flortaucipir BP_{ND} in either grey or white matter or in Flortaucipir spatial extent (Mann-Whitney-Wilcoxon: W=38, P=0.34; W=48, P=0.80; W=44, P=0.60, respectively). Possible interactions between ApoE status (ε4 vs other) and age on Flortaucipir uptake was examined using linear regression. There was a signficant interaction between ApoE genotype and age on Flortaucipir BP_{ND} in the cortical grey matter (χ^2 test, P=0.033), with older individuals carrying at least one ApoE ε4 allele showing higher Flortaucipir cortical uptake. There were no interactions between age and ApoE status on Flortaucipir white matter uptake and on Flortaucipir spatial extent were not statistically significant (P=0.059; P=0.78, respectively).

Off target striatal binding is similar in TBI and healthy controls

In keeping with the known off-target binding of Flortaucipir to neuromelanin *(13)* Flortaucipir BP_{ND} was increased in the striatum in both TBI participants and in

healthy controls when compared to the rest of the cerebral white and grey matter, excluding focal lesions (Wilcoxon signed-rank patients: V=214, P=0.0002; controls: V=66, P=0.001;). However, Flortaucipir BP_{ND} within the striatum was not significantly different between TBI participants and healthy controls (Mann-Whitney-Wilcoxon W=110, P=0.85).

Discussion

Hyperphosphorylated tau deposition is a key pathological feature of neurodegeneration triggered by traumatic brain injury (TBI) *(3, 4)*. Patients are at increased risk of Alzheimer's disease (AD) and chronic traumatic encephalopathy (CTE) after TBI, both characterised by the accumulation of tau pathology. Positron emmission tomography (PET) ligands have recently been developed that specifically bind hyperphosophorylated tau , enabling the detection of tau pathology *in vivo*. We used Flortaucipir PET to investigate tau pathology in a well-characterized cohort of individuals who were examined many years after a single moderate-severe TBI *(24, 25)*. As predicted, there was considerable variability in the extent of Flortaucipir binding across TBI patients. Broadly, a third of patients showed extensive increases in cerebral Flortaucipir binding, a third showed more limited increases and a third showed no abnormality.

Flortaucipir binds to neurofibrillary tangles containing abnormal tau in post-mortem human brain tissue in AD *(13–15)*. A lack of specificity has been a significant issue with previous PET tau ligands *(27)*, but Flortaucipir is more selective and does not show significant β-amyloid, α-synuclein or TDP-43 binding. 'Off-target' binding is present for neuromelanin- and melanin-containing cells, which leads to signal appearing within subcortical structures such as the striatum *(13)*. Flortaucipir has been validated for the study of tau pathology in AD patients, showing binding that correlates with clinical phenotype *(16–18)*, cognitive profile *(16, 17)* and estimated Braak & Braak staging *(19)*. Tau pathology seen after TBI appears to be similar to AD, with all six isoforms of tau (including both 3- and 4-repeat isoforms) observed *(3, 4)*. As a result, Flortaucipir is expected to bind tau pathology seen after TBI in a similar way to AD, albeit with a distinct spatial patern *(3)*.

The pattern of Flortaucipir binding potentially provides diagnostic information about the type of post-traumatic neurodegeneration. Tau pathology seen after TBI often has a distinct distribution from AD. In cases of CTE, tau pathology is concentrated in depths of cortical sulci *(3, 6)* and can be widely distributed in cortical areas following single TBI *(8)*. In line with these pathological findings a number of our patients showed extensive Flortaucipir binding in cortical areas as well as in parts of the white matter. The spatial pattern of Flortaucipir binding would be atypical for

AD *(28)* but is more in keeping with CTE *(3, 4)*. It is also compatible with the spatially extensive tau neurofibrillary tangle pathology seen in approximately one-third of patients studied several years after a single TBI *(8)*.

The relationship between tau pathology and Flortaucipir binding is supported by our cerebrospinal fluid (CSF) results. CSF tau is raised in incipient Alzheimer disease *(29)* and other tauopathies *(30)* and provides a diagnostic biomarker for AD *(31)*. CSF tau increases in the days after TBI, generally falling to normal levels 8-12 weeks after the injury *(32, 33)*. To our knowledge, our study is the first to examine CSF tau several years after moderate-severe TBI. CSF tau was not increased across the TBI group, but there was significant variablity in levels within the group. The variability in cortical Flortaucipir binding correlated with CSF tau. Increased levels of binding were associated with increased CSF tau levels, supporting the the conclusion that increased Flortaucipir binding is indicative of the presence of cortical tau pathology. We also observed a positive correlation between CSF UCH-L1 levels and cortical Flortaucipir uptake. In the acute phase, UCH-L1 provides a biomarker indicating the presence of neuronal injury following TBI *(34)*. It is abundant in cerebral neurons and is an important component of the ubiquitin-proteasome system, *(35)*. Dysfunction of UCH-L1 is implicated in a number of neurodegenerative diseases *(36, 37)* and UCH-L1 is found within misfolded protein aggregates, including neurofibrillary tangles *(38)*. UCH-L1 CSF levels are elevated in patients with Alzheimer disease *(39)* and our results suggest that the link between TBI and dysfunction in the ubiquitin-proteasome system warrants further investigation.

We also showed a relationship between Flortaucipir binding and traumatic axonal injury (TAI), indicated by diffusion tensor imaging and white matter atrophy. Increased Flortaucipir binding was associated with the presence of TAI. This is in keeping with a causative role for TAI in the pathophysiology of post-traumatic tau pathology. Mechanical forces exerted at the time of head injuries are thought to disrupt axonal organization producing damage to microtubule structure and associated axonal tau *(4)*. This damage may lead to hyperphosphorylation of tau, misfolding, and neurofibrillary tangle formation, which eventually causes neurodegeneration *(9, 10, 40)*. Mechanical forces are maximal in points of geometric inflection such as the base of cortical sulci *(41)*, where tau pathtology is seen in CTE.

In AD, increased Flortaucipir binding is greater in cortical regions that show atrophy *(21, 22)*. We observed a slightly different relationship following TBI. White matter Flortaucipir binding was increasd in areas that also showed reduced fractional anisotropy and atrophy. This suggests that tau pathology was more marked in areas of TAI. In addition, cortical Flortaucipir binding also correlated with the extent of TAI within the white matter. For example, Flortaucipir binding in the right lateral occipital cortex, the most consistent area of increase, was correlated with reduced fractional anisotropy - in keeping with TAI - in the inferior longitudinal fasciculus – a tract directly connected to that cortical area. This relationship might be explained by slow Wallerian degeneration that follows the initial injury and leads to the accumulation of tau pathology in connected cortical regions. Alternatively, prion-like spread of tau-pathology might over time result in the cortical accumulation of tau-pathology in regions that are connected to white matter regions initially damage by TAI *(42, 43)*. We have previously reported a similar relationship between cortical amyloid pathology measured using [^{11}C]-PiB PET and the degree of TAI in connected tracts *(44)*, suggesting that the structure of the connectome may influence the location of post-traumatic tau and amyloid pathology in similar ways.

Genetic factors are likely to partly explain the variability in neurodegenerative trajectory following TBI. ApoE ε4, the strongest risk factor for sporadic AD, is associated with increased *β*-amyloid and tau pathology *(45)*. Carrying an ApoE ε4 allele is also associated with poor functional outcome following TBI *(46)*. ApoE ε4 may act synergistically with TBI to elevate the risk of neurodegeneration *(47, 48)*, so we tested the relationship between ApoE status and Flortaucipir binding. Flortaucipir binding was not increased in ApoE ε4 carriers. However ApoE interacted with age, with cortical Flortaucipir binding increasing with age when TBI patients had at least one ε4 allele. In a larger prospective TBI cohort of clinical outcome after TBI, which included some of the participants later recruited to our study, Teasdale and colleagues also showed an interaction between age and ApoE genotype at 6 months post-TBI, with less favourable clinical outcome found in younger ApoE ε4 carriers *(25)*. These results suggest that ApoE ε4 may have a distinct interaction with age depending on whether early clinical or late neurodegenerative associations are being examined. Larger longitudinal studies will be necessary to clarify these relationships.

Our study has a number of limitations, which should be considered. Firstly, the relatively small sample size is likely to have limited our ability to detect associations between Flortaucipir binding and clinical outcomes. We performed a planned comparison of Flortaucipir binding in good and poor outcome subgroups and found no difference in Flortaucipir binding, although both sub-groups showed increased levels of binding. The absence of a clinical effect should be interpreted with caution as our study is unlikely to have been adequately powered for these outcomes. In AD, Flortaucipir uptake was associated with poorer performance in various cognitive domains in regionally specific patterns *(16)*, supporting the hypothesis that a similar relationship may be present following TBI. However, the situation is likely to be more complex following TBI as the influence of the initial injury on cognitive state will confound progressive neurodegenerative effects, meaning that larger sample sizes will be necessary to clarify the relationship between tau pathology and post-traumatic cognitive impairment. Secondly, a minority of subjects were missing longitudinal neuropsychological or CSF data, which will have reduced statistical power with respect to these measures. Thirdly, as previously reported *(13–15, 18, 20, 49)*, Flortaucipir binding shows off-target binding to neuromelanin containing cells, which is particularly apparent in the striatum *(13, 14)*. Off-target binding, albeit to lesser extent, has also been reported in areas of acute parenchymal and subarachnoid haemorrhage, but not in areas showing superficial siderosis due to chronic haemorrhage *(13)*. This is unlikely to be a major confound in our study as there were no acute haemorrhagic lesions in our participants and we observed reduced binding within focal lesions. The off-target Flortaucipir binding may have limited our ability to detect underlying striatal tau pathology due to decreased signal to noise ratio in this region, although this will not have influenced the main cortical and white matter results we report. Finally, there may be concerns about the effect of brain atrophy or reduced tissue density on our PET results. We employed stringent measures to minimise the effects of atrophy during pre-processing. Moreover, the relationship between increased Flortaucipir binding and reduced white matter tissue density is unlikely to be artifactual, as non-specific Flortaucipir binding is expected to be reduced within areas of reduced tissue density, increasing the probabilty of false-negative, not false-positive results.

In summary, we show that Flortaucipir binding is increased many years after a single significant TBI. Increased binding was associated with CSF indicators of neurodegeneration, including tau levels, as well as the presence of TAI that may provide the initial trigger to its accumulation. The ability to detect tau pathology *in vivo* following TBI has major potential implications for diagnosis and prognostication of clinical outcomes after TBI. It is also likely to assist in patient selection and stratification for future treatment trials targeting tau.

Materials and Methods

Study design and participants

Individuals were recruited with a history of a single moderate-severe TBI (according to Mayo classification *(50)*) at least 18 years prior to recruitment, and no prior significant neurological or psychiatric illness, or contraindication to PET or MRI. TBI participants were primarily recruited from a patient cohort under follow-up at the Institute of Health and Wellbeing, Head Injury Research Group, University of Glasgow, UK. These individuals have been followed up longitudinally in terms of cognitive, wellbeing and disability outcomes *(24, 25)*. Additional TBI patients were recruited from the specialist multidisciplinary TBI clinic at Imperial College Healthcare NHS Trust, London, UK. Patients were divided into two subgroups based on functional outcome. Poor functional outcome was defined as a GOS-E score of 6 or less (moderate-severe disability) at the time of assessment and those with GOS-E greater than 6 as good outcome. Healthy volunteers of similar age and socioeconomic background as the TBI participants were also recruited. The study was approved by the Westminster Research Ethics Committee and the Administration of Radioactive Substances Advisory Committee. All participants gave written informed consent.

Procedures

All participants were administered an IV bolus of Flortaucipir (also known as [^{18}F]AV-1451 and [^{18}F]T807), average dose 250 MBq and dynamic PET scans were acquired over 90 minutes. Flortaucipir was supplied by Avid Radiopharmaceuticals, a wholly owned subsidiary of Eli Lilly and Company and PET image acquisition was carried out at Imanova Centre for Imaging Sciences. All participants also underwent structural 3T MRI, including volumetric T1 and diffusion tensor imaging (DTI). Diffusion-weighted images were acquired along 64 non-collinear directions with b=1000s/mm^2 and four averages with b=0s/mm2, with TE/TR 103/9,500ms, 64 contiguous slices, FoV 256 mm, and voxel size 2×2×2 mm^3.

TBI participants and healthy controls took part in neuropsychological assessment focusing on cognitive domains often impaired after TBI (Table 2) *(44, 51)*. The Wechsler Test of Adult Reading (WTAR) estimated pre-morbid

intelligence; the Wechsler Abbreviated Scale of Intelligence (WASI) Matrix Reasoning subtest assessed non-verbal reasoning; a tablet computer-based left/right choice-reaction task (CRT) measured processing speed (median reaction time (RT) on correct trials); complex processing speed and executive function was assessed with the Colour-Word Interference (Stroop) subtests from the Delis-Kaplan Executive Function System (inhibition and cognitive flexibility) and the Trail Making Test (TMT) (set maintenance and set shifting); a tablet computer-based paired associates learning (PAL) test assessed associative working memory; the People Test from the Doors and People Test assessed episodic memory; the Hopkins Verbal Learning Test (HVLT) assessed verbal immediate and delayed recall; visuospatial immediate and delayed recall were assessed using the Brief Visuospatial Memory Test (BVMT); complex visual perception was assessed using the tablet computer-based Feature Match test. Participants also completed a Mini-Mental State Examination (MMSE).

TBI and control participants had venous blood and cerebrospinal fluid (CSF) sampling. Clinical assessment, blood and CSF sample acquisition were carried out at the NIHR/Welcome Trust Imperial Clinical Research Facility.

Biomarker and genetic analyses

Microtubule-associated tau concentration was measured in plasma and CSF using the Human Total Tau kit (Quanterix, Boston, MA) with the Simoa HD-1 Analyzer (Quanterix, Boston, MA). Briefly, samples, magnetic beads coated with Tau5 monoclonal capture antibody, and HT7 & BT2 monoclonal biotinylated detector antibodies were combined. Antibody epitopes in the mid-region of tau make the assay sensitive to normal and phosphorylated tau, including most of the known protein isoforms.

Additionally, four biomarkers of axonal damage and neuronal degeneration *(52)* were mesured in plasma and CSF both in TBI and healthy controls using the Simoa Human Neurology 4-Plex Aassay (N4PA; Quanterix): ubiquitin carboxy-terminal hydrolase L1 (UCH-L1), neurofilament light (NFL), glial fibrillary acidic protein (GFAP), and protein S100.

Apolipoprotein E (ApoE) genotyping was performed on peripheral blood. DNA was extracted using the Qiagen QIAamp DNA blood mini kit. Genotyping of the c.388T>C p (SNP.rs429358) and the c.526C>T (SNP.rs7412) of the ApoE gene was performed using a TaqMan Allelic Discrimination assay.

PET image processing

Image preprocessing and model fitting of the Flortaucipir PET data was performed using the Molecular Imaging and Kinetic Analysis Toolbox (MIAKAT™, www.miakat.org). Motion correction of the dynamic PET images was performed with frame-by-frame correction using rigid body registration to a reference frame. The motion-corrected PET images were then registered to the individual's T1 MRI image with a rigid-body registration resulting in a motion-corrected dynamic PET image in individual T1 space.

The dynamic PET data was analysed using the simplified reference tissue model (SRTM) *(53, 54)*. Cerebellar grey matter was chosen as the reference tissue, based on post-mortem studies in chronic traumatic encephalopathy which demonstrated relative sparing from tau pathology in that region *(3, 7)*. The reference region was defined as follows. Structural MR images were segmented using the unified segmentation algorithm in SPM12 *(55)* to produce grey matter probability maps. Voxels exceeding a grey matter tissue probability of at least 0.9 were considered to be grey matter, to ensure only voxels corresponding to healthy grey matter were included in the reference region. The grey matter and white matter probability maps were subsequently used to create DARTEL *(56)* flow fields from subject space to MNI152 space. The inverse mappings of these flow fields were applied to the CIC atlas *(57)* to produce an atlas image in each individuals' MR structural T1 space. The grey matter cerebellum reference region was defined as the intersection of the grey matter voxels (tissue probability of 0.9 or greater) and the voxels in the cerebellum ROI in the subject space atlas.

Time activity curves (TAC) were generated for the reference region defined for each subject by plotting the mean intensity of the voxels in the reference region for each frame. Using this TAC as reference, SRTM was fitted at the voxel level to generate parametric images of Flortaucipir non-displaceable binding potential

(BP_{ND}). Flortaucipir BP_{ND} parametric images were normalised to MNI152 space using the previously derived DARTEL flow fields from subject space to MNI152 space. The flow fields were applied to the BP_{ND} parametric images without modulation using a 8mm full width at half maximum (FWHM) Gaussian smoothing kernel.

To obtain a quantitative spatial measure of Flortaucipir binding in each individual patient as compared to healthy controls, voxelwise z-scores of MNI registered BP_{ND} images were derived for each patient versus the healthy control group. The spatially normalised BP_{ND} images were used to create a z-score image for each of the 21 TBI patients based on the mean and standard deviation of the group of the 11 healthy controls at each voxel. For comparison, z-score images were also computed for each healthy control versus the group of the remaining 10 healthy controls. The number of voxels with BP_{ND} $z>1.645$ (corresponding to $P<0.05$ 1-tailed) was used as a summary measure of the spatial extent of increased Flortaucipir signal for each participant.

MRI lesion segmentation

Structural MRI scans of all participants were reviewed by a senior neuroradiologist. Focal lesions apparent on T1 MRI were manually segmented in individual T1 space. Individual lesion maps were registered to MNI152 standard space using affine linear registration in FSL *(58)* and a 4mm FWHM Gaussian smoothing kernel was applied to these spatially normalised lesion maps to account for partial volume effects when applying the lesion maps to PET images. In individuals with focal lesions, BP_{ND} within lesions was compared to BP_{ND} in the rest of the cerebrum, excluding the striatum (where off-target binding was observed). Individual subjects' lesions were excluded from voxelwise permutation analyses by incorporating a tool which uses voxels corresponding to individual lesions as voxelwise regressors in the general linear model (GLM).

MRI processing

Voxel-based morphometry was performed on volumetric T1 MRI images *(59)*. T1 images were segmented into grey and white matter using SPM12 *(55)*, and warped to an average group template using the diffeomorphic nonlinear registration (DARTEL) algorithm *(56)* then the individual flow-fields and template transformation from DARTEL were applied to produce MNI space images. No modulation was applied after spatial normalisation, therefore the resulting spatial maps represent tissue concentration (grey or white matter density), rather than volume *(59, 60)*. Normalized grey and white matter density maps were spatially smoothed (8mm full width at half maximum (FWHM) Gaussian kernel).

Diffusion-weighted images were preprocessed using standard methods *(61)* and tensor-based registration performed using DTI-TK *(62)*. Fractional anisotropy (FA) maps were generated and registered for group analyses using tract-based spatial statistics (TBSS) *(63)*.

Statistical analyses

Statistical analyses were carried out in the R statistical software (www.r-project.org) *(64)* unless specified otherwise. Deviation from normal distribution was examined for all variables using the Shapiro-Wilk test and Q-Q plots. Two-tailed t-tests and Mann-Whitney tests were used for between-group comparisons, as appropriate.

Voxelwise differences in BP_{ND} between TBI participants and healthy controls, between each of the disabled TBI and good recovery TBI subgroups and healthy controls as well as between these subgroups were assessed using permutation tests in FSL *(65)*. The same procedure was used to assess voxelwise differences between patients and controls in: i) VBM-derived white matter density ii) grey matter density and iii) diffusion MRI-derived skeletonised fractional anisotropy (FA). Voxels corresponding to structural lesions were excluded from the analyses by using subjects' lesion maps as individual voxelwise repressors. All cerebral grey and white matter voxels were included except those corresponding to the striatum, where there is known off-target binding *(13)*. 1000 permutations were used and results were cluster-corrected for multiple comparisons using threshold-free cluster enhancement (TFCE) and a family-wise error rate of 0.05. Localisation of significant voxel clusters

was reported based on the Harvard-Oxford probabilistic atlas *(66)* and the JHU DTI-based white matter atlas *(67)*.

To investigate whether white matter tau pathology shared common localisation with traumatic axonal injury and / or white matter atrophy in TBI, we compared skeletonized FA and, separately, average white matter density (z-scores) within areas of high Flortaucipir signal (BP_{ND} $z>1.645$) versus white matter areas where binding was not increased (BP_{ND} $z<1.645$) using (paired) Wilcoxon signed-rank tests. Any voxels corresponding to focal lesions were excluded. Only TBI participants with 15 or more white matter voxels with increased Flortaucipir binding within the regions of interest were included.

To examine the localisation of white matter microstructural damage predicted by increased Flortaucipir cortical signal in TBI participants, standardized BP_{ND} within the right parietal cortical area of significant Flortaucipir increase in TBI was used as a regressor in a voxelwise GLM of skeletonised FA, and separately, in a voxelwise GLM of white matter density. Statistical significance was tested using permutation tests in FSL *(65)*. As previously, voxels corresponding to lesions were excluded for each individual, 1000 permutations were used and results were obtained using TFCE, corrected for multiple comparisons using a family-wise error rate of 0.05. Localisation of significant voxel clusters was reported based on the JHU DTI-based white matter atlas *(67)*. Post-hoc correlations were examined using Spearman's rank correlation between standardized BP_{ND} within the right parietal cortical area of significant Flortaucipir increase in TBI participants and skeletonized FA in the following tracts: right and left superior longitudinal, inferior longitudinal, inferior fronto-occipital fasiculi and cingulum bundles, corpus callosum (genu, body and splenium) as well as in the right and left corticospinal tracts as a control.

Correlations between clinical/neuropsychological measures and PET markers in TBI participants were examined using Spearman's rank correlation with false discovery rate (FDR) correction for multiple comparisons. Interactions between ApoE and age were assessed by comparing two linear regression models, with and without the interaction term, using chi squared test. Assumptions of multiple linear regression analysis were tested as follows: analysis of standard residuals was carried out to identify outliers; variance inflation factor was used to test for multicollinearity;

Durbin-Watson test was conducted to test for independence of errors; approximate normal distribution of errors, homoscedacity and linearity were assessed by plotting regression standardized residuals.

Supplementary Materials

Fig. S1. Focal lesions in TBI participants.

Table S1. Correlations between Flortaucipir right parietal cluster (TBI>Control) BP_{ND} (z-score compared to healthy controls) and FA in white matter tracts in TBI patients.

Table S2. Correlations between clinical measures and each of: Flortaucipir right parietal cluster (TBI>Control) BP_{ND}, whole cerebral cortex BP_{ND} (z-score compared to the healthy control group), white matter BP_{ND} (z-score compared to the healthy control group) and spatial extent (N of voxels with BP_{ND} z-score>1.645 of healthy controls) in TBI patients.

References and Notes

1. D. H. Smith, V. E. Johnson, W. Stewart, Chronic neuropathologies of single and repetitive TBI: substrates of dementia?, *Nature Reviews Neurology* **9**, 211–221 (2013).

2. S. Fleminger, D. L. Oliver, S. Lovestone, S. Rabe-Hesketh, A. Giora, Head injury as a risk factor for Alzheimer's disease: the evidence 10 years on; a partial replication, *Journal of Neurology, Neurosurgery & Psychiatry* **74**, 857–862 (2003).

3. A. C. McKee, T. D. Stein, C. J. Nowinski, R. A. Stern, D. H. Daneshvar, V. E. Alvarez, H.-S. Lee, G. Hall, S. M. Wojtowicz, C. M. Baugh, D. O. Riley, C. A. Kubilus, K. A. Cormier, M. A. Jacobs, B. R. Martin, C. R. Abraham, T. Ikezu, R. R. Reichard, B. L. Wolozin, A. E. Budson, L. E. Goldstein, N. W. Kowall, R. C. Cantu, The spectrum of disease in chronic traumatic encephalopathy, *Brain* **136**, 43–64 (2013).

4. K. Blennow, J. Hardy, H. Zetterberg, The neuropathology and neurobiology of traumatic brain injury, *Neuron* **76**, 886–899 (2012).

5. J. a. N. Corsellis, C. J. Bruton, D. Freeman-Browne, The aftermath of boxing, *Psychological Medicine* **3**, 270–303 (1973).

6. A. C. McKee, N. J. Cairns, D. W. Dickson, R. D. Folkerth, C. D. Keene, I. Litvan, D. P. Perl, T. D. Stein, J.-P. Vonsattel, W. Stewart, Y. Tripodis, J. F. Crary, K. F. Bieniek, K. Dams-O'Connor, V. E. Alvarez, W. A. Gordon, the T. Group, The first NINDS/NIBIB consensus meeting to define neuropathological criteria for the diagnosis of chronic traumatic encephalopathy, *Acta Neuropathol* **131**, 75–86 (2016).

7. J. Mez, D. H. Daneshvar, P. T. Kiernan, B. Abdolmohammadi, V. E. Alvarez, B. R. Huber, M. L. Alosco, T. M. Solomon, C. J. Nowinski, L. McHale, K. A. Cormier, C. A. Kubilus, B. M. Martin, L. Murphy, C. M. Baugh, P. H. Montenigro, C. E. Chaisson, Y. Tripodis, N. W. Kowall, J. Weuve, M. D. McClean, R. C. Cantu, L. E. Goldstein, D. I. Katz, R. A. Stern, T. D. Stein, A. C. McKee, Clinicopathological Evaluation of Chronic Traumatic Encephalopathy in Players of American Football, *JAMA* **318**, 360–370 (2017).

8. V. E. Johnson, W. Stewart, D. H. Smith, Widespread Tau and Amyloid- Beta Pathology Many Years After a Single Traumatic Brain Injury in Humans, *Brain Pathology* **22**, 142–149 (2012).

9. H. T. Tran, F. M. LaFerla, D. M. Holtzman, D. L. Brody, Controlled cortical impact traumatic brain injury in 3xTg-AD mice causes acute intra-axonal amyloid-β accumulation and independently accelerates the development of tau abnormalities, *Journal of Neuroscience* **31**, 9513–9525 (2011).

10. H. T. Tran, L. Sanchez, D. L. Brody, Inhibition of JNK by a peptide inhibitor reduces traumatic brain injury–induced tauopathy in transgenic mice, *Journal of Neuropathology & Experimental Neurology* **71**, 116–129 (2012).

11. C.-F. Xia, J. Arteaga, G. Chen, U. Gangadharmath, L. F. Gomez, D. Kasi, C. Lam, Q. Liang, C. Liu, V. P. Mocharla, F. Mu, A. Sinha, H. Su, A. K. Szardenings, J. C. Walsh, E. Wang, C. Yu, W. Zhang, T. Zhao, H. C. Kolb, [18F]T807, a novel tau positron emission tomography imaging agent for Alzheimer's disease, *Alzheimer's & Dementia: The Journal of the Alzheimer's Association* **9**, 666–676 (2013).

12. D. T. Chien, A. K. Szardenings, S. Bahri, J. C. Walsh, F. Mu, C. Xia, W. R. Shankle, A. J. Lerner, M.-Y. Su, A. Elizarov, Early clinical PET imaging results with the novel PHF-tau radioligand [F18]-T808, *Journal of Alzheimer's Disease* **38**, 171–184 (2014).

13. M. Marquié, M. D. Normandin, C. R. Vanderburg, I. M. Costantino, E. A. Bien, L. G. Rycyna, W. E. Klunk, C. A. Mathis, M. D. Ikonomovic, M. L. Debnath, N. Vasdev, B. C. Dickerson, S. N. Gomperts, J. H. Growdon, K. A. Johnson, M. P. Frosch, B. T. Hyman, T. Gómez-Isla, Validating

novel tau positron emission tomography tracer [F-18]-AV-1451 (T807) on postmortem brain tissue, *Ann Neurol.* **78**, 787–800 (2015).

14. K. Sander, T. Lashley, P. Gami, T. Gendron, M. F. Lythgoe, J. D. Rohrer, J. M. Schott, T. Revesz, N. C. Fox, E. \AArstad, Characterization of tau positron emission tomography tracer [18 F] AV-1451 binding to postmortem tissue in Alzheimer's disease, primary tauopathies, and other dementias, *Alzheimer's & Dementia* **12**, 1116–1124 (2016).

15. M. Marquié, M. D. Normandin, A. C. Meltzer, M. Siao Tick Chong, N. V. Andrea, A. Antón-Fernández, W. E. Klunk, C. A. Mathis, M. D. Ikonomovic, M. Debnath, others, Pathological correlations of [F-18]-AV-1451 imaging in non-alzheimer tauopathies, *Annals of neurology* **81**, 117–128 (2017).

16. R. Ossenkoppele, D. R. Schonhaut, M. Schöll, S. N. Lockhart, N. Ayakta, S. L. Baker, J. P. O'Neil, M. Janabi, A. Lazaris, A. Cantwell, others, Tau PET patterns mirror clinical and neuroanatomical variability in Alzheimer's disease, *Brain* **139**, 1551–1567 (2016).

17. D. Tosun, S. Landau, P. S. Aisen, R. C. Petersen, M. Mintun, W. Jagust, M. W. Weiner, A. D. N. Initiative, Association between tau deposition and antecedent amyloid-β accumulation rates in normal and early symptomatic individuals, *Brain* **140**, 1499–1512 (2017).

18. L. Passamonti, P. Vázquez Rodríguez, Y. T. Hong, K. S. Allinson, D. Williamson, R. J. Borchert, S. Sami, T. E. Cope, W. R. Bevan-Jones, P. S. Jones, others, 18F-AV-1451 positron emission tomography in Alzheimer's disease and progressive supranuclear palsy, *Brain* **140**, 781–791 (2017).

19. A. J. Schwarz, P. Yu, B. B. Miller, S. Shcherbinin, J. Dickson, M. Navitsky, A. D. Joshi, M. D. Devous Sr, M. S. Mintun, Regional profiles of the candidate tau PET ligand 18 F-AV-1451 recapitulate key features of Braak histopathological stages, *Brain* **139**, 1539–1550 (2016).

20. R. Smith, A. Puschmann, M. Schöll, T. Ohlsson, J. Van Swieten, M. Honer, E. Englund, O. Hansson, 18F-AV-1451 tau PET imaging correlates strongly with tau neuropathology in MAPT mutation carriers, *Brain* **139**, 2372–2379 (2016).

21. C. Xia, S. J. Makaretz, C. Caso, S. McGinnis, S. N. Gomperts, J. Sepulcre, T. Gomez-Isla, B. T. Hyman, A. Schultz, N. Vasdev, others, Association of in vivo [18F] AV-1451 tau PET imaging results with cortical atrophy and symptoms in typical and atypical Alzheimer disease, *Jama neurology* **74**, 427–436 (2017).

22. L. Wang, T. L. Benzinger, Y. Su, J. Christensen, K. Friedrichsen, P. Aldea, J. McConathy, N. J. Cairns, A. M. Fagan, J. C. Morris, others, Evaluation of tau imaging in staging Alzheimer disease and revealing interactions between β-amyloid and tauopathy, *JAMA neurology* **73**, 1070–1077 (2016).

23. D. L. Dickstein, M. Y. Pullman, C. Fernandez, J. A. Short, L. Kostakoglu, K. Knesaurek, L. Soleimani, B. D. Jordan, W. A. Gordon, K. Dams-O'Connor, B. N. Delman, E. Wong, C. Y. Tang, S. T. DeKosky, J. R. Stone, R. C. Cantu, M. Sano, P. R. Hof, S. Gandy, Cerebral [18 F]T807/AV1451 retention pattern in clinically probable CTE resembles pathognomonic distribution of CTE tauopathy, *Transl Psychiatry* **6**, e900 (2016).

24. G. M. Teasdale, G. D. Murray, J. a. R. Nicoll, The association between APOE ε4, age and outcome after head injury: a prospective cohort study, *Brain* **128**, 2556–2561 (2005).

25. K. Millar, J. A. R. Nicoll, S. Thornhill, G. D. Murray, G. M. Teasdale, Long term neuropsychological outcome after head injury: relation to APOE genotype, *Journal of Neurology, Neurosurgery & Psychiatry* **74**, 1047–1052 (2003).

26. D. J. Sharp, G. Scott, R. Leech, Network dysfunction after traumatic brain injury, *Nature Reviews. Neurology* **10**, 156 (2014).

27. E. D. Agdeppa, V. Kepe, J. Liu, S. Flores-Torres, N. Satyamurthy, A. Petric, G. M. Cole, G. W. Small, S.-C. Huang, J. R. Barrio, Binding Characteristics of Radiofluorinated 6-Dialkylamino-2-Naphthylethylidene Derivatives as Positron Emission Tomography Imaging Probes for β-Amyloid Plaques in Alzheimer's Disease, *J. Neurosci.* **21**, RC189–RC189 (2001).

28. H. Braak, E. Braak, Staging of alzheimer's disease-related neurofibrillary changes, *Neurobiology of Aging* **16**, 271–278 (1995).

29. O. Hansson, H. Zetterberg, P. Buchhave, E. Londos, K. Blennow, L. Minthon, Association between CSF biomarkers and incipient Alzheimer's disease in patients with mild cognitive impairment: a follow-up study, *The Lancet Neurology* **5**, 228–234 (2006).

30. M. B. Aerts, R. a. J. Esselink, B. R. Bloem, M. M. Verbeek, Cerebrospinal fluid tau and phosphorylated tau protein are elevated in corticobasal syndrome, *Mov. Disord.* **26**, 169–173 (2011).

31. N. Andreasen, L. Minthon, P. Davidsson, E. Vanmechelen, H. Vanderstichele, B. Winblad, K. Blennow, Evaluation of CSF-tau and CSF-Aβ42 as diagnostic markers for Alzheimer disease in clinical practice, *Archives of Neurology* **58**, 373–379 (2001).

32. H. Zetterberg, M. A. Hietala, M. Jonsson, N. Andreasen, E. Styrud, I. Karlsson, \AAke Edman, C. Popa, A. Rasulzada, L.-O. Wahlund, Neurochemical aftermath of amateur boxing, *Archives of neurology* **63**, 1277–1280 (2006).

33. G. Franz, R. Beer, A. Kampfl, K. Engelhardt, E. Schmutzhard, H. Ulmer, F. Deisenhammer, Amyloid beta 1-42 and tau in cerebrospinal fluid after severe traumatic brain injury, *Neurology* **60**, 1457–1461 (2003).

34. L. Papa, L. M. Lewis, S. Silvestri, J. L. Falk, P. Giordano, G. M. Brophy, J. A. Demery, M. C. Liu, J. Mo, L. Akinyi, S. Mondello, K. Schmid, C. S. Robertson, F. C. Tortella, R. L. Hayes, K. K. W. Wang, Serum levels of Ubiquitin C-terminal Hydrolase (UCH-L1) distinguish mild traumatic brain injury (TBI) from trauma controls and are elevated in mild and moderate TBI patients with intracranial lesions and neurosurgical intervention, *J Trauma Acute Care Surg* **72**, 1335–1344 (2012).

35. K. D. Wilkinson, K. M. Lee, S. Deshpande, P. Duerksen-Hughes, J. M. Boss, J. Pohl, The neuron-specific protein PGP 9.5 is a ubiquitin carboxyl-terminal hydrolase, *Science* **246**, 670–673 (1989).

36. K. Bilguvar, N. K. Tyagi, C. Ozkara, B. Tuysuz, M. Bakircioglu, M. Choi, S. Delil, A. O. Caglayan, J. F. Baranoski, O. Erturk, C. Yalcinkaya, M. Karacorlu, A. Dincer, M. H. Johnson, S. Mane, S. S. Chandra, A. Louvi, T. J. Boggon, R. P. Lifton, A. L. Horwich, M. Gunel, Recessive loss of function of the neuronal ubiquitin hydrolase UCHL1 leads to early-onset progressive neurodegeneration, *PNAS* **110**, 3489–3494 (2013).

37. J. Choi, A. I. Levey, S. T. Weintraub, H. D. Rees, M. Gearing, L.-S. Chin, L. Li, Oxidative modifications and down-regulation of ubiquitin carboxyl-terminal hydrolase L1 associated with idiopathic Parkinson's and Alzheimer's diseases, *J. Biol. Chem.* **279**, 13256–13264 (2004).

38. J. Lowe, H. McDermott, M. Landon, R. J. Mayer, K. D. Wilkinson, Ubiquitin carboxyl-terminal hydrolase (PGP 9.5) is selectively present in ubiquitinated inclusion bodies characteristic of human neurodegenerative diseases, *The Journal of Pathology* **161**, 153–160 (1990).

39. A. Öhrfelt, P. Johansson, A. Wallin, U. Andreasson, H. Zetterberg, K. Blennow, J. Svensson, Increased Cerebrospinal Fluid Levels of Ubiquitin Carboxyl-Terminal Hydrolase L1 in Patients with Alzheimer's Disease, *DEE* **6**, 283–294 (2016).

40. Y. Yoshiyama, K. Uryu, M. Higuchi, L. Longhi, R. Hoover, S. Fujimoto, T. McIntosh, V. M.-Y. Lee, J. Q. Trojanowski, Enhanced neurofibrillary tangle formation, cerebral atrophy, and cognitive deficits induced by repetitive mild brain injury in a transgenic tauopathy mouse model, *Journal of neurotrauma* **22**, 1134–1141 (2005).

41. M. Ghajari, P. J. Hellyer, D. J. Sharp, Computational modelling of traumatic brain injury predicts the location of chronic traumatic encephalopathy pathology, *Brain* **140**, 333–343 (2017).

42. M. G. Spillantini, M. Goedert, Tau pathology and neurodegeneration, *The Lancet Neurology* **12**, 609–622 (2013).

43. M. Polymenidou, D. W. Cleveland, Prion-like spread of protein aggregates in neurodegeneration, *Journal of Experimental Medicine* **209**, 889–893 (2012).

44. G. Scott, A. F. Ramlackhansingh, P. Edison, P. Hellyer, J. Cole, M. Veronese, R. Leech, R. J. Greenwood, F. E. Turkheimer, S. M. Gentleman, R. A. Heckemann, P. M. Matthews, D. J. Brooks, D. J. Sharp, Amyloid pathology and axonal injury after brain trauma, *Neurology* **86**, 821–828 (2016).

45. Y. Shi, K. Yamada, S. A. Liddelow, S. T. Smith, L. Zhao, W. Luo, R. M. Tsai, S. Spina, L. T. Grinberg, J. C. Rojas, G. Gallardo, K. Wang, J. Roh, G. Robinson, M. B. Finn, H. Jiang, P. M. Sullivan, C. Baufeld, M. W. Wood, C. Sutphen, L. McCue, C. Xiong, J. L. Del-Aguila, J. C. Morris, C. Cruchaga, Alzheimer's Disease Neuroimaging Initiative, A. M. Fagan, B. L. Miller, A. L. Boxer, W. W. Seeley, O. Butovsky, B. A. Barres, S. M. Paul, D. M. Holtzman, ApoE4 markedly exacerbates tau-mediated neurodegeneration in a mouse model of tauopathy, *Nature* **549**, 523–527 (2017).

46. L. Li, Y. Bao, S. He, G. Wang, Y. Guan, D. Ma, R. Wu, P. Wang, X. Huang, S. Tao, Q. Liu, Y. Wang, J. Yang, The Association Between Apolipoprotein E and Functional Outcome After Traumatic Brain Injury, *Medicine (Baltimore)* **94** (2015).

47. J. A. R. Nicoll, G. W. Roberts, D. I. Graham, Apolipoprotein E ε4 allele is associated with deposition of amyloid β-protein following head injury, *Nature Medicine* **1**, 135–137 (1995).

48. V. E. Johnson, W. Stewart, D. H. Smith, Traumatic brain injury and amyloid-β pathology: a link to Alzheimer's disease?, *Nature Reviews Neuroscience* **11**, 361–370 (2010).

49. M. Schöll, S. N. Lockhart, D. R. Schonhaut, J. P. O'Neil, M. Janabi, R. Ossenkoppele, S. L. Baker, J. W. Vogel, J. Faria, H. D. Schwimmer, others, PET imaging of tau deposition in the aging human brain, *Neuron* **89**, 971–982 (2016).

50. J. F. Malec, A. W. Brown, C. L. Leibson, J. T. Flaada, J. N. Mandrekar, N. N. Diehl, P. K. Perkins, The Mayo classification system for traumatic brain injury severity, *Journal of neurotrauma* **24**, 1417–1424 (2007).

51. A. F. Ramlackhansingh, D. J. Brooks, R. J. Greenwood, S. K. Bose, F. E. Turkheimer, K. M. Kinnunen, S. Gentleman, R. A. Heckemann, K. Gunanayagam, G. Gelosa, D. J. Sharp, Inflammation after trauma: Microglial activation and traumatic brain injury, *Ann Neurol.* **70**, 374–383 (2011).

52. H. Zetterberg, K. Blennow, Fluid biomarkers for mild traumatic brain injury and related conditions, *Nature Reviews Neurology* **12**, 563–574 (2016).

53. A. A. Lammertsma, S. P. Hume, Simplified Reference Tissue Model for PET Receptor Studies, *NeuroImage* **4**, 153–158 (1996).

54. R. N. Gunn, A. A. Lammertsma, S. P. Hume, V. J. Cunningham, Parametric Imaging of Ligand-Receptor Binding in PET Using a Simplified Reference Region Model, *NeuroImage* **6**, 279–287 (1997).

55. J. Ashburner, K. J. Friston, Unified segmentation, *NeuroImage* **26**, 839–851 (2005).

56. J. Ashburner, A fast diffeomorphic image registration algorithm, *NeuroImage* **38**, 95–113 (2007).

57. A. C. Tziortzi, G. E. Searle, S. Tzimopoulou, C. Salinas, J. D. Beaver, M. Jenkinson, M. Laruelle, E. A. Rabiner, R. N. Gunn, Imaging dopamine receptors in humans with [11C]-(+)-PHNO: Dissection of D3 signal and anatomy, *NeuroImage* **54**, 264–277 (2011).

58. M. Jenkinson, P. Bannister, M. Brady, S. Smith, Improved Optimization for the Robust and Accurate Linear Registration and Motion Correction of Brain Images, *NeuroImage* **17**, 825–841 (2002).

59. J. Ashburner, K. J. Friston, Voxel-Based Morphometry—The Methods, *NeuroImage* **11**, 805–821 (2000).

60. A. Mechelli, C. J. Price, K. J. Friston, J. Ashburner, Voxel-based morphometry of the human brain: methods and applications, *Current medical imaging reviews* **1**, 105–113 (2005).

61. K. M. Kinnunen, R. Greenwood, J. H. Powell, R. Leech, P. C. Hawkins, V. Bonnelle, M. C. Patel, S. J. Counsell, D. J. Sharp, White matter damage and cognitive impairment after traumatic brain injury, *Brain* **134**, 449–463 (2011).

62. H. Zhang, B. B. Avants, P. A. Yushkevich, J. H. Woo, S. Wang, L. F. McCluskey, L. B. Elman, E. R. Melhem, J. C. Gee, High-Dimensional Spatial Normalization of Diffusion Tensor Images Improves the Detection of White Matter Differences: An Example Study Using Amyotrophic Lateral Sclerosis, *IEEE Transactions on Medical Imaging* **26**, 1585–1597 (2007).

63. S. M. Smith, M. Jenkinson, H. Johansen-Berg, D. Rueckert, T. E. Nichols, C. E. Mackay, K. E. Watkins, O. Ciccarelli, M. Z. Cader, P. M. Matthews, others, Tract-based spatial statistics: voxelwise analysis of multi-subject diffusion data, *Neuroimage* **31**, 1487–1505 (2006).

64. R Core Team, others, R: A language and environment for statistical computing, (2014) (available at http://www.R-project.org/).

65. A. M. Winkler, G. R. Ridgway, M. A. Webster, S. M. Smith, T. E. Nichols, Permutation inference for the general linear model, *NeuroImage* **92**, 381–397 (2014).

66. R. S. Desikan, F. Ségonne, B. Fischl, B. T. Quinn, B. C. Dickerson, D. Blacker, R. L. Buckner, A. M. Dale, R. P. Maguire, B. T. Hyman, An automated labeling system for subdividing the human cerebral cortex on MRI scans into gyral based regions of interest, *Neuroimage* **31**, 968–980 (2006).

67. K. Hua, J. Zhang, S. Wakana, H. Jiang, X. Li, D. S. Reich, P. A. Calabresi, J. J. Pekar, P. C. van Zijl, S. Mori, Tract probability maps in stereotaxic spaces: analyses of white matter anatomy and tract-specific quantification, *Neuroimage* **39**, 336–347 (2008).

Acknowledgments:

Funding: Medical Research Council (MRC) UK grant number: MR/L022141/1. UK Dementia Research Institute (PMM). National Institute of Health Research (NIHR) UK (DJS). Academy of Medical Sciences (NG).

Author contributions: NG: acquisition, analysis and interpretation of data, drafting and critical revision of the article, final approval of the version to be published; LML: acquisition, analysis and interpretation of data, critical revision of the article, final approval of the version to be published; AW: analysis and interpretation of data, drafting and critical revision of the article, final approval of the version to be published; KAZ: acquisition of data, critical revision of the article, final approval of the version to be published; LM: acquisition of data, critical revision of the article, final approval of the version to be published; CML: acquisition of data, critical revision of the article, final approval of the version to be published; AH: analysis of data, critical revision of the article, final approval of the version to be published; HZ: design and interpretation of data, critical revision of the article, final approval of the version to be published; JP: design and interpretation of data, critical revision of the article, final approval of the version to be published; PMM: design and interpretation of data, critical revision of the article, final approval of the version to be published; RNG: design and interpretation of data, critical revision of the article, final approval of the version to be published; TMM: design and interpretation of data, critical revision of the article, final approval of the version to be published; DJS: conception and design of the study, interpretation of data, drafting and critical revision of the article, final approval of the version to be published.

Competing interests: None declared

Supplementary Materials:

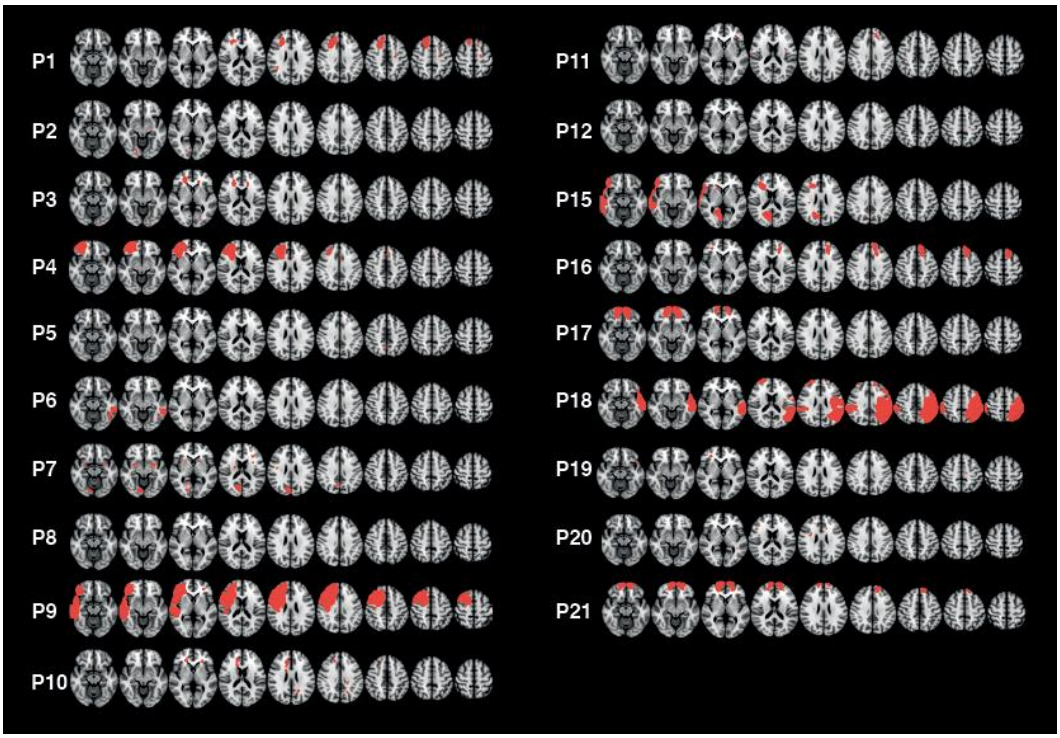

Fig. S1: Focal lesions in TBI participants. Axial MRI slices of focal lesions (radiological convention). Patient labels correspond to those in Table 1 and Fig. 1-2. Participants P13 and P14 are not included as they did not have a focal lesion.

White matter tract FA		Right parietal ROI Flortaucipir BP_{ND} z-score	
		ρ	P
Cingulum bundle	Right	**-0.68**	**<0.001**
	Left	-0.37	0.10
Inferior longitudinal fasciculus	Right	**-0.44**	**0.049**
	Left	-0.27	0.23
Inferior fronto-occipital fasciculus	Right	-0.41	0.067
	Left	-0.36	0.11
Superior longitudinal fasciculus	Right	-0.20	0.38
	Left	-0.06	0.79
Anterior thalamic radiation	Right	**-0.54**	**0.011**
	Left	-0.26	0.24
Uncinate fasciculus	Right	**-0.47**	**0.033**

	Left	-0.04	0.85
Corpus callosum	Genu	**-0.68**	**<0.001**
	Body	**-0.44**	**0.047**
	Splenium	-0.31	0.17
Corticospinal tract	Right	-0.01	0.96
	Left	-0.29	0.21

Table S1: Correlations between Flortaucipir right parietal cluster (TBI>Control) BP_{ND} (z-score compared to healthy controls) and FA in white matter tracts in TBI patients. Spearman rho coefficients and P-values are presented, P<0.05 in bold.

	Outcome measure	R parietal ROI Flortaucipir BP_{ND} z-score		Grey matter Flortaucipir BP_{ND} z-score		White matter Flortaucipir BP_{ND} z-score		Flortaucipir spatial extent	
		ρ	P	ρ	P	ρ	P	ρ	P
Age **(years)**		-0.15	0.53	0.01	0.96	-0.11	0.65	0.11	0.62
Time since injury **(years)**		0.15	0.52	-0.02	0.94	-0.01	0.95	0.18	0.44
Disability	GOS-E (current)	-0.40	0.072	-0.02	0.92	-0.15	0.52	-0.33	0.15
	GOS-E (change)	-0.25	0.37	-0.28	0.31	-0.47	0.075	-0.19	0.50
Cognitive impairment	MMSE (current)	-0.32	0.16	-0.06	0.81	-0.04	0.85	-0.18	0.43
	MMSE (change)	-0.34	0.24	-0.31	0.28	-015	0.62	-0.29	0.31
Logical reasoning	WASI Matrix Reasoning	**-0.50**	**0.019**	-0.01	0.96	-0.01	0.96	-0.22	0.33
Processing speed	Trail Making Test A	0.22	0.36	0.11	0.64	0.12	0.61	0.33	0.16
	Trail Making Test B	0.23	0.33	0.11	0.64	0.13	0.56	0.42	0.06
	Stroop Combined Baseline	-0.08	0.74	-0.05	0.81	0.02	0.93	-0.08	0.72
	CRT RT	**0.50**	**0.024**	0.29	0.19	0.25	0.28	**0.51**	**0.01**
Executive function	Trail Making Test B-A	0.13	0.59	0.08	0.73	0.10	0.67	0.37	0.11
	Stroop Inhibition-Switch	0.21	0.37	-0.009	0.97	0.009	0.97	0.17	0.47
	Stroop Inhibition-Switch vs Baseline	0.04	0.87	-0.22	0.34	-0.20	0.39	-0.01	0.96
	FrSBe-Executive; current	0.06	0.81	-0.002	0.99	0.08	0.72	0.19	0.41
Apathy	LARS	0.14	0.55	-0.07	0.77	-0.005	0.98	0.23	0.33

	FrSBe-Apathy; current	0.06	0.80	-0.07	0.76	-0.008	0.97	0.26	0.25
Impulsivity / Disinhibition	BIS	0.31	0.19	-0.09	0.70	0	1	0.06	0.81
	FrSBe-Disinhibition; current	0.19	0.41	0.14	0.53	0.23	0.31	0.26	0.26
Verbal memory	DaPT People Immediate Recall	-0.23	0.28	-0.05	0.81	0.02	0.94	-0.03	0.91
	DaPT People Delayed Recall	-0.33	0.15	-0.04	0.86	0.06	0.81	0.06	0.81
	HVLT Immediate Recall	-0.23	0.32	-0.13	0.58	-0.15	0.51	-0.24	0.29
	HVLT Delayed Recall	-0.27	0.24	-0.23	0.32	-0.20	0.39	-0.30	0.19
	HVLT RDI	-0.31	0.17	-0.27	0.23	-0.20	0.39	-0.35	0.12
Visual memory	Paired Associates Learning	-0.13	0.58	0.06	0.79	-0.02	0.93	-0.13	0.58
	STMBT Binding Accuracy	-0.38	0.16	-0.14	0.62	-0.19	0.50	-0.28	0.32
	BVMT Immediate Recall	-0.37	0.10	0.003	0.99	-0.08	0.72	-0.19	0.41
	BVMT Delayed Recall	-0.37	0.10	-0.11	0.63	-0.10	0.65	-0.24	0.30
	BVMT RDI	-0.18	0.45	-0.02	0.94	-0.001	0.99	-0.21	0.36
Visuospatial ability	Feature match test	-0.34	0.14	0	1	-0.16	0.49	-0.21	0.35
Mood disturbance	HADS-Anxiety	0.38	0.091	0.01	0.96	0.09	0.70	0.18	0.44
	HADS-Depression	0.18	0.44	-0.21	0.36	-0.17	0.47	0.14	0.53

Abbreviations: BIS = Barratt Impulsivity Scale; BVMT = Brief Visuospatial Memory Test; CRT = Choice reaction time; DaPT = Doors and People's Test; FrSBe = Frontal Systems Behavior Scale; GOS-E = Glasgow Outcome Scale – Extended; HADS = Hospital Anxiety and Depression Score; HVLT = Hopkins Verbal Learning Test; LARS = Lille Apathy Rating Scale; MMSE = Mini-mental State Examination; ms = milliseconds; RDI = Recognition Discrimination Index; RT = Reaction time; s = seconds; SD = Standard deviation; STBMT = Short Term Memory Binding Test; WASI = Wechsler Abbreviated Scale for Intelligence; WTAR = Wechsler Test of Adult Reading.

Table S2: Correlations between clinical measures and each of: Flortaucipir right parietal cluster (TBI>Control) BP_{ND}, whole cerebral cortex BP_{ND} (z-score compared to the healthy control group), white matter BP_{ND} (z-score compared to the healthy control group) and spatial extent (N of voxels with BP_{ND} z-score>1.645 of healthy controls) in TBI patients. Spearman ρ coefficients and uncorrected P-values (P<0.05 in bold) are presented; all P>0.05 following FDR adjustment for multiple comparisons.